International Core Journal of Engineering Volume 10 Issue 10, 2024
ISSN: 2414-1895 DOI: 10.6919/ICJE.202410_10(10).0014

The Effect of Annealing on the Microstructure and Properties of the $Zr_xAlCoCrFeNi_{2.1}$ High-Entropy Alloy

Weichu Sun[a], Zhijun Cheng[b]

School of Materials and Chemistry, University of Shanghai for Science and Technology, Shanghai 200093, China

[a]903589083@qq.com, [b]623667044@qq.com

Abstract

The $Zr_xAlCoCrFeNi_{2.1}$ eutectic high-entropy alloys (x=0, 0.01, 0.05, 0.1) were prepared using the vacuum electric furnace melting method and subjected to annealing at 600°C for 12 hours. The microstructural changes of the alloys with zirconium addition were analyzed using X-ray diffraction, scanning electron microscopy, and energy dispersive spectroscopy. Additionally, the Vickers hardness and room temperature compressive properties of the $Zr_xAlCoCrFeNi_{2.1}$ alloys were tested.The results indicate that $AlCoCrFeNi_{2.1}$ is a eutectic high-entropy alloy, primarily composed of FCC and B2 phases, with the FCC phase being dominant. As the zirconium content increases, nickel elements gradually precipitate from the B2 phase, forming Ni_7Zr_2 (Laves phase), which distributes in a network structure between the FCC and B2 phases. This structural change significantly enhances the hardness and compressive strength of the alloy.However, excessive zirconium leads to the coarsening of phases in the alloy, reducing the precipitation strengthening effect and resulting in a decrease in hardness and compressive performance. Overall, the main strengthening mechanisms of the alloy with increasing zirconium content are the precipitation strengthening from the hard Laves phase and the solid solution strengthening working in synergy.In summary, an appropriate amount of zirconium addition can effectively improve the properties of the $Zr_xAlCoCrFeNi_{2.1}$ alloy, while excessive zirconium can negatively impact the mechanical properties of the alloy.

Keywords

High-Entropy Alloys; Zr Content; Microstructure; Mechanical Properties.

1. Introduction

In recent decades, high-entropy alloys (HEAs) have attracted widespread attention as a new material system due to their multi-principal-element design and excellent properties. These alloys are typically composed of five or more principal elements in equiatomic ratios, forming simple solid solution structures rather than complex intermetallic compounds. The $Zr_xAlCoCrFeNi_{2.1}$ high-entropy alloy, as a representative of this category, has become a research hotspot due to its outstanding performance in mechanical properties, oxidation resistance, and corrosion resistance. In this alloy system, the elements work together through complex solid solution strengthening mechanisms, significantly enhancing the material's strength and hardness. Additionally, the high-entropy effect reduces the atomic diffusion rate in the crystal structure, allowing the alloy to exhibit excellent thermal stability in high-temperature environments.

For the $Zr_xAlCoCrFeNi_{2.1}$ alloy, the addition of Zr not only helps to further improve its oxidation resistance in high-temperature environments but may also alter its phase composition and

ISSN: 2414-1895 DOI: 10.6919/ICJE.202410_10(10).0014

microstructure, thereby affecting its mechanical properties. Existing studies have shown that the addition of Zr can promote the formation of more stable body-centered cubic (BCC) or face-centered cubic (FCC) structures to some extent, both of which are beneficial for enhancing the overall mechanical performance and environmental tolerance of the material[1][2]. Furthermore, research on the $Zr_xAlCoCrFeNi_{2.1}$ alloy provides new insights into the development of high-entropy alloys. Specifically, by adjusting the Zr content, the phase structure and phase composition of the alloy can be significantly altered. For instance, at higher Zr concentrations, the alloy may form a more complex multiphase structure, which could include nanoscale precipitates that significantly enhance the strength and hardness of the material[3]. Meanwhile, the formation of these phases also helps to impede dislocation movement, further improving the mechanical performance of the alloy. On the other hand, the addition of Zr can significantly enhance the alloy's corrosion resistance, especially in harsh high-temperature oxidation environments, providing important theoretical and technical support for its applications in fields such as nuclear energy and aerospace[4]. In summary, the $ZrAlCoCrFeNi_{2.1}$ high-entropy alloy achieves optimization of microstructure and macroscopic performance through multi-element alloy design, laying a solid foundation for the development of the next generation of high-performance alloy materials. Therefore, this study utilizes vacuum arc melting to prepare a series of $Zr_xAlCoCrFeNi_{2.1}$ (x=0, 0.01, 0.05, 0.1) high-entropy alloy ingots by adding Zr to the $AlCoCrFeNi_{2.1}$ eutectic high-entropy alloy, and investigates the microstructure and mechanical properties of the $Zr_xAlCoCrFeNi_{2.1}$ series alloys after annealing treatment.

2. Experiment

2.1 Materials and Methods

In this experiment, high-purity (99.99 wt.%) Al, Co, Cr, Fe, Ni, and Zr bulk materials were used as raw materials. Under argon protection, $Zr_xAlCoCrFeNi_{2.1}$ (x: molar ratio, x=0, 0.01, 0.05, and 0.1) high-entropy alloys were prepared using cold crucible floating melting. To ensure the chemical uniformity of the ingots, each alloy was remelted at least five times, and the purity of the alloy elements was not lower than 99.9 wt.%. The samples were heated in an N61/H-type muffle furnace at a heating rate of 10°C/min to 600°C, held for 12 hours, and then air-cooled to room temperature.

Phase analysis was conducted using a Bruker D8 X-ray diffractometer (XRD) equipped with a Cu target, with a scanning range of 20° to 95°. After polishing the samples with SiC sandpaper, they were finely polished using a 1.5 μm diamond suspension and then etched with a mixed solution of nitric acid and hydrochloric acid in a volume ratio of 1:3 for 30 seconds. The microstructure of the alloy was observed using a S-3400N tungsten filament scanning electron microscope (SEM), and the alloy composition was determined using the energy-dispersive spectrometer (EDS) and back-scattered electron (BSE) detector attached to the SEM.Wire cutting was used to obtain samples measuring Φ 10 mm × 10 mm × 2 mm, and hardness measurements were conducted on the alloy using an HXD-1000 digital microhardness tester, with a test load of 100 gf and a holding time of 10 seconds. The room temperature compression performance of the alloy was tested using a Gleeble 3180 thermal simulation testing machine, with samples sized Φ 3 mm × 6 mm in cylindrical form, a strain rate of 1×10^{-3} s^{-1}, and a strain of 0.5.

3. Results and Discussion

3.1 Microstructure and Phase Constitution of $Zr_xAlCoCrFeNi_{2.1}$

Figure 1 shows the XRD patterns of the cast $Zr_xAlCoCrFeNi_{2.1}$ high-entropy alloys (x = 0, 0.01, 0.05, 0.1) and the diffraction peaks of the (111) crystal plane. The research results indicate that when x = 0, the alloy exhibits a dual-phase structure of FCC + B2 (see Figure 1a). When x = 0.01, no new diffraction peaks are observed. As the Zr content increases to x = 0.05 and x = 0.1, diffraction peaks of the Ni_7Zr_2 phase appear at 2θ = 35.88° (100) and 2θ = 64.82° (001). Further analysis reveals that the intensity of the diffraction peaks varies with different Zr contents. From Figure 1(b), it can be seen that as Zr is added, the intensity of the diffraction peak for the (111) crystal plane first decreases

ISSN: 2414-1895 DOI: 10.6919/ICJE.202410_10(10).0014

and then increases. When the Zr content reaches a certain level, new diffraction peaks corresponding to the Laves phase appear, indicating that the B2 structure in the solid solution phase gradually precipitates Laves phase, leading to an increase in the proportion of the Laves phase and a decrease in the proportion of the B2 phase. At the same time, Zr atoms exist in the FCC matrix in the form of interstitial solid solution, which gradually enhances the intensity of the (111) crystal plane diffraction peak. As the Zr content increases, the zirconium compounds gradually precipitate, causing the diffraction peaks to shift to larger angles.

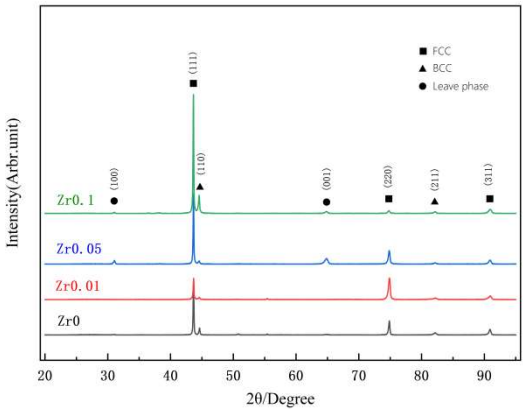

Figure 1. XRD pattern of $Zr_xAlCoCrFeNi_{2.1}$ HEAs after heat treatment.

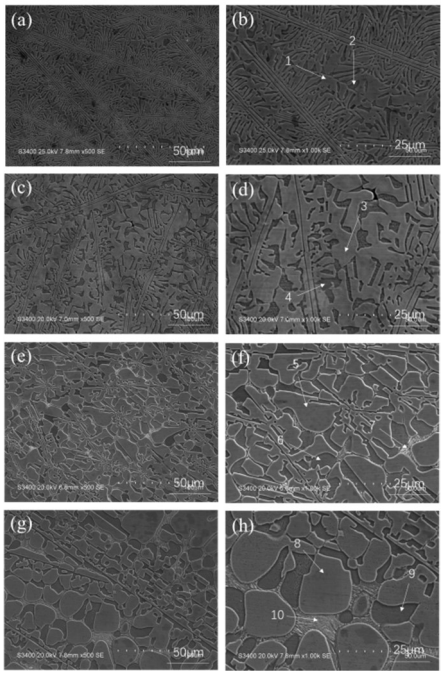

Figure 2. SEM images of $Zr_xAlCoCrFeNi_{2.1}$ HEAs after heat treatment show:, (b) x=0; (c), (d) x=0.01; (e), (f) x=0.05; (g), (h) x=0.1

Figure 2shows the SEM images of $Zr_xAlCoCrFeNi_{2.1}$ high-entropy alloy. In the absence of Zr, as shown in Figure 2(a), the alloy mainly consists of FCC + B2 phases, exhibiting a layered morphology. When the Zr content increases to x = 0.01, Figure 2(c) reveals that the microstructure of the alloy consists of both layered and petal-like structures. The FCC phase structure transitions from a sheet-like to a petal-like form, accompanied by some degree of coarsening and dissolution, but no precipitates are observed (Figure 2(d)). This is attributed to the very low content of Zr at this stage; during the solidification process, Zr dissolves into the FCC + B2 phases, inducing lattice distortion

ISSN: 2414-1895 DOI: 10.6919/ICJE.202410_10(10).0014

and altering the phase structure of the alloy, while no significant precipitate phase is generated.As the Zr content further increases to x = 0.05, a significant change in the alloy's structure is observed, as shown in Figure 2(e). The layered and petal-like structures completely transform into petal-like structures, and zirconides gradually precipitate between the FCC and B2 phases. These zirconides mainly appear as white particles and are concentrated at the grain boundaries, forming a discontinuous network structure, as seen in Figure 2(f). This phenomenon occurs because the primary FCC + B2 phases solidify first during the solidification process, while the secondary zirconides solidify later in the residual liquid. Over time, the primary phase gradually pushes the secondary phase to the grain boundaries, resulting in the concentration of zirconides in these regions.When the Zr content increases to x = 0.1 (Figures 2(g) and (h)), it is evident that the petal-like morphology further enlarges, and the amount of zirconides aggregated at the phase boundaries increases, evolving from the discontinuous network structure in Figure 2(e) to a continuous network structure in Figure 2(g).

Table 1. Chemical composition distribution of as-cast

	No.	Elements					
		Al	Co	Cr	Fe	Ni	Zr
X=0	1(BCC)	22.35	14.95	15.25	14.98	32.47	—
	2(FCC)	10.45	17.27	20.75	18.07	33.47	—
X=0.01	3(BCC)	23.51	13.42	11.71	11.49	39.63	0.25
	4(FCC)	12.40	17.57	19.07	18.16	32.68	0.12
X=0.05	5(BCC)	26.15	13.16	10.03	11.39	38.95	0.32
	6(FCC)	11.64	18.29	18.90	19.00	31.96	0.20
	7(Laves)	12.05	15.30	12.25	12.14	40.41	7.84
X=0.1	8(BCC)	26.67	12.98	10.04	11.21	38.65	0.45
	9(FCC)	11.00	18.49	20.11	19.77	30.51	0.13
	10(Laves)	9.58	15.51	10.44	10.94	43.37	10.52

To further clarify the phase composition of alloys with different Zr contents, micro-area compositional analysis was conducted using Energy Dispersive Spectroscopy (EDS). Table 2 presents the composition of each element in the high-entropy alloy along with the EDS analysis results. In the absence of zirconium, the composition within grain area 1 in Figure 2(b) is not significantly different from the nominal composition. Combined with the XRD results, area 1 corresponds to the B2-based phase, while area 2 corresponds to the FCC-based phase. As the amount of Zr elements added gradually increases, the data in Table 1, along with areas 7 and 10 in Figure 2, indicate that the newly formed phase in Figure 2 is rich in Ni and Zr, with a ratio of approximately 7:2. Thus, it can be inferred that the precipitate phase in Figure 2 is Ni_7Zr_2, which is consistent with the results obtained from XRD.Figure 3 shows the elemental mapping distribution of $Zr_xAlCoCrFeNi_{2.1}$high-entropy alloy. It can be observed that the elements Al, Co, Cr, Fe, and Ni in the $AlCoCrFeNi_{2.1}$ alloy are distributed relatively uniformly, with almost no compositional segregation, as shown in Figure 3(a). After adding Zr to the alloy, Figures 3(b), (c), and (d) show that the matrix FCC phase is rich in Al and Ni, while the matrix B2 phase is rich in Co, Cr, and Fe. The particulate and network precipitate phases are rich in Ni and Zr[5]. At the onset of solidification, a small amount of Zr preferentially dissolves into the FCC + B2 phases, but due to the limited solubility of Zr, as the zirconium content continues to increase, it is expelled to the phase boundary regions, forming a Zr-rich zone. With further increases in Zr content, a small amount of Zr dissolves into the

ISSN: 2414-1895 DOI: 10.6919/ICJE.202410_10(10).0014

FCC and B2 phases, while the remaining Zr is added to the $AlCoCrFeNi_{2.1}$ alloy, forming a Zr-rich Laves phase. When Zr content further increases to x = 0.05, particles rich in Ni and Zr precipitate at the phase boundaries, and a connecting Zr-rich zone forms between the particles, presenting a vague discontinuous network structure, as seen in Figures 3(c). As the Zr content ultimately increases to x = 0.1, the precipitate phases connect into a continuous network structure.Al and Ni elements have very negative mixing enthalpies and share the same crystal structure, which allows them to easily substitute for other elements in their respective lattice positions and exhibit better compatibility, potentially leading to the enrichment of Al and Ni in the B2 phase[6]. Co, Cr, and Fe elements have similar atomic radii and strong chemical compatibility, forming FCC phases rich in Co, Cr, and Fe[7]. The radius ratio of Zr to the elements in the $AlFeCrCoNi_{2.1}$ high-entropy alloy is R_{Zr}/R_{Co}=1.28, R_{Zr}/R_{Ni}=1.29, R_{Zr}/R_{Al}=1.12, R_{Zr}/R_{Cr}=1.25, R_{Zr}/R_{Fe},=1.27, indicating they are quite similar. From the perspective of electronegativity, the electronegativity of Ni is 1.91, which is significantly higher than that of the other elements in the alloy, while Zr is the element with the lowest electronegativity in the alloy. The greater the electronegativity of an element, the stronger its tendency to attract other electrons. Among the elements in the alloy, Ni has relatively high electronegativity, while Zr has the lowest. Additionally, the atomic radius of Zr is very similar to that of Ni, making their combination more favorable for the formation of Ni_7Zr_2.

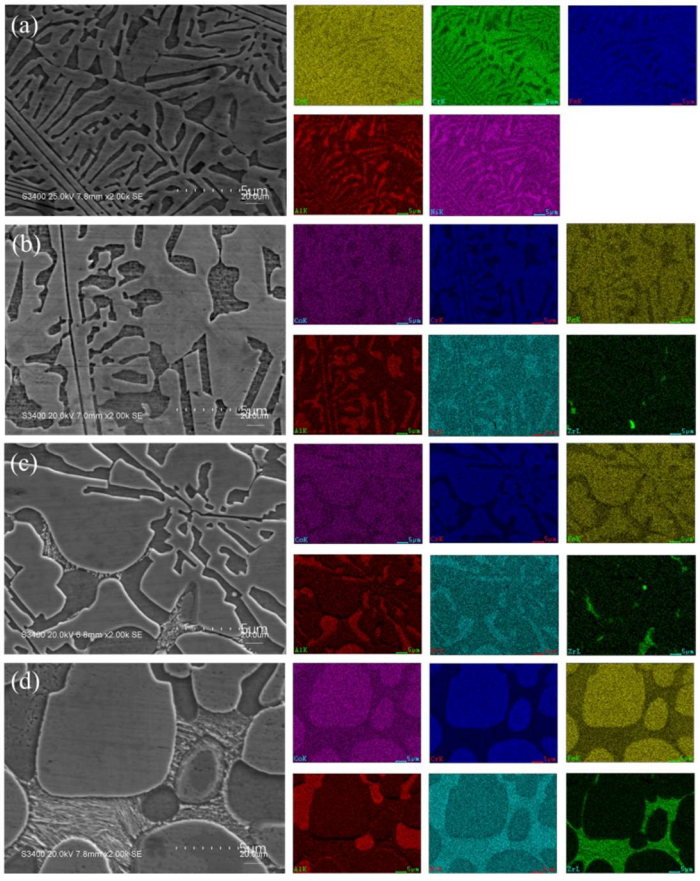

Figure 3. EDS mapping images of $Zr_xAlCoCrFeNi_{2.1}$ HEAs after heat treatment: (a) x = 0; (b) x = 0.01; (c) x = 0.05; (a) x = 0.1

3.2 Mechanical Properties of $Zr_xAlCoCrFeNi_{2.1}$

Figure 4 illustrates the average hardness and corresponding indentation morphology of the cast $Zr_xAlCoCrFeNi_{2.1}$ high-entropy alloy. The figure indicates that as the Zr content increases, the hardness initially rises and then declines. At a Zr content of x = 0.05, the hardness reaches its peak value of 368.1 HV. This increase in hardness can be attributed to the lattice distortion caused by the addition of Zr, which enhances solid solution strengthening.Furthermore, XRD and EDS analyses

ISSN: 2414-1895 DOI: 10.6919/ICJE.202410_10(10).0014

reveal that as Zr content increases, some Zr reacts with Ni elements in the B2 phase to form Ni_7Zr_2, further enhancing the alloy's hardness through precipitation strengthening. However, when the Zr content rises to x = 0.1, the alloy's phase structure changes, as depicted in Figures 2(b) and 2(h). The structure transitions from a lamellar form to a petal-like structure, characterized by coarse Laves phase grain boundaries. This alteration not only weakens the grain boundaries but also depletes strengthening elements such as Ni and Al from the matrix (Figure 2(d)), diminishing the effects of both solid solution strengthening and precipitation strengthening, which ultimately leads to a reduction in hardness[8].

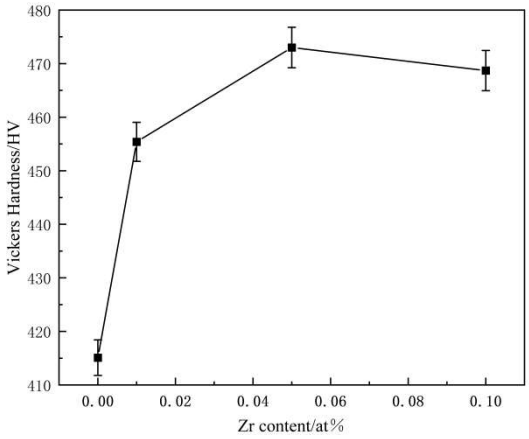

Figure 4. Average Vickers hardness and indentation morphology of $Zr_xAlCoCrFeNi_{2.1}$ HEAs after heat treatment.

Figure 5 shows the true stress-strain curves of the as-cast $Zr_xAlCoCrFeNi_{2.1}$ high-entropy alloy after annealing. From the figure, it can be observed that as the Zr content increases, the slope of the curve increases, indicating that the elastic modulus of the alloy is continuously increasing. Simultaneously, the compressive strength of the alloy is also improving with the deformation amount. However, the fracture strain of the alloy decreases to varying degrees with the addition of different amounts of Zr, indicating a reduction in the alloy's plasticity.When x = 0.01, the addition of Zr significantly enhances the solid solution strengthening effect, leading to an increase in the alloy's strength. When the Zr content reaches x = 0.05, the compressive strength of the alloy drops to 2069.3 MPa. This is mainly due to the formation of a network-like Laves phase in the alloy, which increases the resistance to dislocation slip during compressive deformation, thereby enhancing the alloy's strength. When x = 0.1, the performance of the alloy deteriorates, with both strength and plasticity significantly declining. This is because the excessive addition of Zr reduces the number of solid solutions in the alloy, diminishing the effect of solid solution strengthening. Additionally, excessive Zr can form brittle Laves phases at the grain boundaries, leading to embrittlement of the grain boundaries, which in turn reduces the toughness and strength of the alloy. Literature has indicated that excessively high Zr content may adversely affect the thermal processing and formability of the alloy, as Zr reduces the alloy's plasticity and workability[9]. In industrial production, too high a Zr content may also lead to casting defects, thus affecting the formability and quality of the alloy.The yield strength of the alloy after annealing shows a consistent trend with the compressive strength, reaching a maximum of 1301.4 MPa at x = 0.01. Overall, $Zr_xAlCoCrFeNi_{2.1}$ (x = 0, 0.01, 0.05, 0.1) high-entropy alloys can exhibit various effects such as solid solution strengthening and second-phase strengthening after annealing. Adding an appropriate amount of Zr to the equiatomic $AlCoCrFeNi_{2.1}$ high-entropy alloy can slightly enhance the overall performance of the alloy after annealing. However, for alloys with high Zr content, the formation of hard brittle phases in the alloy microstructure after annealing significantly reduces the alloy's strength and toughness.

ISSN: 2414-1895 DOI: 10.6919/ICJE.202410_10(10).0014

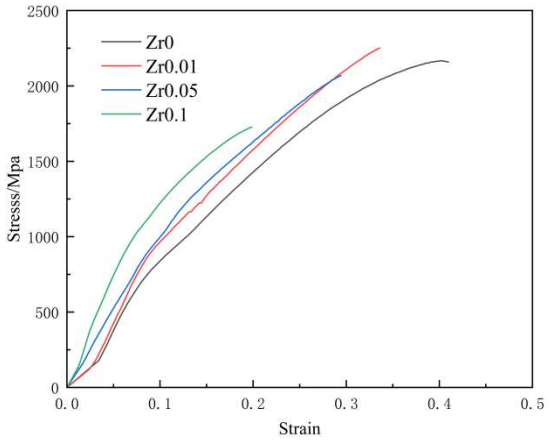

Figure 5. True stress-strain curves for $Zr_xAlCoCrFeNi_{2.1}$ HEAs after heat treatment.

Table 2. Compressive mechanical properties ($\sigma_{0.2}$-yield strength, σ_c-compressive strength) of $Zr_xAlCoCrFeNi_{2.1}$ HEAs after heat treatment.

Strength/MPa	x = 0	x = 0.01	x = 0.05	x = 0.1
$\sigma_{0.2}$	1098.3	1012.7	1301.4	1225.6
σ_c	2167.0	2069.3	2251.3	1726.8

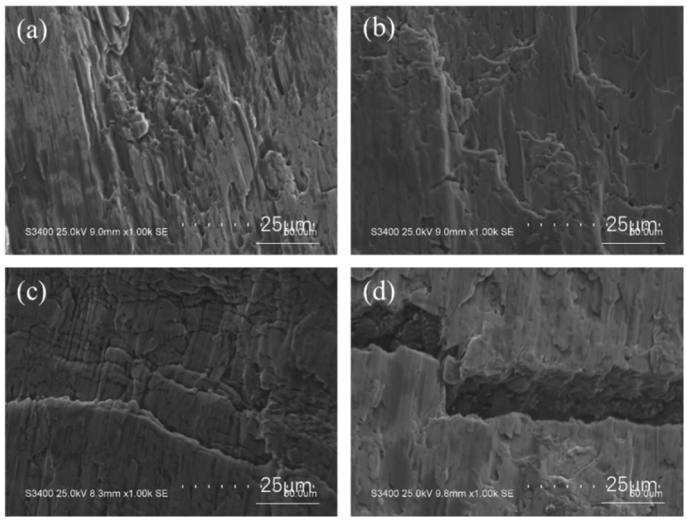

Figure 6. Compression fracture morphology of annealed $Zr_xAlCoCrFeNi_{2.1}$ high-entropy alloy: x=0, (b) x=0.01, (c) x=0.05, (d) x=0.1

In Figure 6, it can be observed that when x = 0, the fracture surface of the alloy exhibits a large number of dimples, and slip phenomena are clearly visible[10]. This is a typical quasi-cleavage fracture with very low plasticity, characteristic of brittle fracture. This is consistent with the previously measured results. For the alloy at x = 0.01, the macro fracture of the alloy specimen occurs along a 45° cross-section, with a reduction in the number of dimples on the microscopic fracture surface, indicating a decrease in the alloy's plasticity. At x = 0.05, the fracture surface of the alloy is flat and smooth, exhibiting cleavage facets, which indicates brittle cleavage fracture. When x = 0.1, secondary cracks appear on the fracture surface, which remains bright and smooth, also showing distinct step-like features, further confirming the poor plasticity of the alloy.

ISSN: 2414-1895 DOI: 10.6919/ICJE.202410_10(10).0014

4. Conclusion

(1) In the Zr-containing alloys, the FCC phase is enriched with Co, Cr, and Fe elements, the B2 phase is enriched with Al and Ni elements, and the Laves phase is enriched with Zr and Ni elements. As the Zr content increases, the microstructure of the alloy gradually changes from a lamellar structure to a petal-like structure. With the increase in Zr content, the Laves phase (Ni_7Zr_2) gradually precipitates from the B2 phase, leading to a continuous decrease in the B2 phase and an increase in the Laves phase. At x = 0.01, the Laves phase exhibits a granular dispersed distribution; at x = 0.05, it shows a discontinuous network distribution; and at x = 0.1, it transforms into a continuous network distribution.

(2) With the increase in Zr content, the hardness of the alloy shows an overall upward trend, reaching a maximum value of 473 HV at x = 0.05, which is an increase of approximately 14%. However, there is no significant improvement in the yield strength and compressive strength of the alloy; on the contrary, the toughness of the alloy decreases significantly. At x = 0.1, the strength of the alloy decreases by about 440 MPa compared to the alloy without Zr, indicating that annealing is detrimental to the improvement of the alloy's compressive performance.

References

[1] Cantor, B., Chang, I. T. H., Knight, P., & Vincent, A. J. B. Microstructural development in equiatomic multicomponent alloys. Materials Science and Engineering: A, 2004,375–377: 213–218.

[2] Miracle, D. B., & Senkov, O. N. (2017). A critical review of high entropy alloys and related concepts. Acta Materialia, 122, 448-511.

[3] Zhang, Y., Zuo, T. T., Tang, Z., Gao, M. C., Dahmen, K. A., Liaw, P. K., & Lu, Z. P. Microstructures and properties of high-entropy alloys. Progress in Materials Science, 2014,61:1-93.

[4] George, E. P., Raabe, D., & Ritchie, R. O. High-entropy alloys. Nature Reviews Materials, 2019,4(8): 515-534.

[5] Chen Jian, Niu Pengyun, Liu Yunzi, et al. Effect of Zr content on microstructure and mechanical properties of AICoCrFeNi high entropy alloy[J]. Materials Design. 2016, 94 (6) : 39-44.

[6] Xie H B , Liu G Z , Guo J J, et al.Effects of Mn, V, Mo, Ti, Zr elements on microstructure and high temperature oxidation performance of AlFeCrCoCu-X high-entropy alloys[J].The Chinese Journal of Nonferrous Metals, 2015, 25 (1): 103-110.

[7] Lu Y , Gao X , Jiang L ,et al. Directly cast bulk eutectic and near-eutectic high entropy alloys with balanced strength and ductility in a wide temperature range[J]. Acta Materialia, 2017, 124: 143-150.

[8] Gu Baolan, Liu Jiachen, Sun Haoyu, Liu Wang, Yu Haiyang. Behavior of grain boundary precipitates of P91 steel during creep process[J]. Heat Treatment of Metals, 2023, 48(5): 25-31.

[9] Zhu Jiawu, Ouyang Sheng. Effect of annealing on microstructure, mechanical properties and magnetic properties of FeCoNi2-xMnGax high-entropy alloys[J]. Heat Treatment of Metals, 2024, 49(1): 22-31.

[10] Xian X , Zhong Z , Zhang B ,et al.A high-entropy V_(35)Ti_(35)Fe_(15)Cr_(10)Zr_5 alloy with excellent high-temperature strength[J].Materials & Design, 2017, 121(MAY):229-236.